RSC Advances

PAPER

View Article Online
View Journal | View Issue

Cite this: *RSC Adv.*, 2017, **7**, 52414

Syngas production: diverse H_2/CO range by regulating carbonates electrolyte composition from CO_2/H_2O *via* co-electrolysis in eutectic molten salts†

Yue Liu, ‡[a] Dandan Yuan, ‡[a] Deqiang Ji,[a] Zhida Li,[a] Zhonghai Zhang,[b] Baohui Wang[a] and Hongjun Wu *[a]

Received 3rd July 2017
Accepted 31st October 2017

DOI: 10.1039/c7ra07320h

rsc.li/rsc-advances

We present a novel sustainable method for the direct production of syngas (H_2 + CO) from CO_2/H_2O co-electrolysis using a hermetic device, to address the continuously increasing level of environmental carbon dioxide (CO_2). All experiments were conducted using a two-electrode system with a coiled Fe cathode and coiled Ni anode in eutectic mixtures of binary and ternary carbonates with hydroxide in a 0.1 : 1 hydroxide/carbonate ratio. With an applied voltage of 1.6–2.6 V and an operating temperature of 500–600 °C, the H_2/CO product ratio was easily tuned from 0.53 to 8.08 through renewable cycling of CO_2 and H_2O. The $Li_{0.85}Na_{0.61}K_{0.54}CO_3$–0.1LiOH composite had the highest current efficiency among those tested, with an optimum value approaching ~93%. This study provides a promising technique for the electrochemical conversion of CO_2/H_2O to a controllable syngas feedstock that can be used in a broad range of industrial applications.

Introduction

The ever-increasing combustion of non-renewable fossil fuels due to industrial development is releasing a large amount of carbon dioxide (CO_2) into the atmosphere, which has led to a serious greenhouse effect. As CO_2 is the main component of greenhouse gases, effectively controlling CO_2 generation and emission are urgent issues.[1–3] Using photochemical and electrochemical methods for the chemical reduction of CO_2 to reverse oxidative degradation is a huge challenge.[4–10] Among current technologies, chemical conversion and utilization of CO_2 is the most promising because it is both an economic and environmental friendly option. Since the last century, there has been gratifying progress in research on CO_2 chemical conversion, especially with respect to the electrode materials, electrolytes, and operating conditions required for electrochemical reduction in molten salts.[11–18] Syngas, a mixture of carbon monoxide (CO) and hydrogen (H_2), has been cited as an essential precursor to a wide range of high value-added industrial products, such as olefins, fuels, and additives. Conventional syngas production methods include natural gas conversion, heavy oil conversion, and folding airflow bed gasification technology.[19–21] However, the high temperatures (over 800 °C) required inevitably consume heat and promote reactor corrosion.[22] In comparison, the molten salt electrolysis technique reported herein provides a low-temperature, stable, and safe route to syngas production.

In this method, the source of hydrogen (H_2) in syngas is LiOH, while carbon monoxide (CO) is sourced from carbonates. The co-electrolysis of CO_2/H_2O in eutectic molten salts provides a feasible way to produce syngas, which can be used in the Fischer–Tropsch (F–T) process to convert electrical energy to chemical energy.[23] Syngas with a H_2/CO ratio of 1.7–3.1 was obtained by controlling the H_2O/CO_2 feed ratio, as reported by Lee.[24] Recently, Sastre *et al.* developed an electrochemical method for converting CO_2 and H_2O into syngas using a nanostructured Ag/g-C_3N_4 catalyst, with H_2/CO ratios ranging from 100 : 1 to 2 : 1.[25] We also demonstrated that, by rational design of the molten salt mixture, a desirable lower temperature (such as 600 °C) led to the highly efficient one-pot generation of syngas *via* CO_2/H_2O coelectrolysis with a current efficiency of ~92% and a H_2/CO ratio of 1.96–7.97 in $Li_{1.07}Na_{0.75}Ca_{0.045}CO_3$/0.15LiOH electrolyte.[22] This result demonstrates that $CaCO_3$ addition affects the composition of syngas. Using these methods, the CO_2/H_2O-derived generation of syngas has been achieved. Although syngas has successfully been produced in previous studies using a molten salt medium, H_2 is the favored product, often resulting in a H_2/CO molar ratio greater than 1.

[a]*Provincial Key Laboratory of Oil & Gas Chemical Technology, College of Chemistry & Chemical Engineering, Northeast Petroleum University, Daqing 163318, China. E-mail: hjwu@nepu.edu.cn; hjwu1979@163.com*

[b]*Department of Chemistry, East China Normal University, 500 Dongchuan Road, Shanghai, 200241, China*

† Electronic supplementary information (ESI) available. See DOI: 10.1039/c7ra07320h

‡ The two authors contributed equally to this paper.

However, there are specific reactions in which a H_2/CO molar ratio of less than 1 is needed, such as in alcohol synthesis with a H_2/CO ratio of 0.5–2 using K/Cu/Co/Zn/Al catalyst.[26] To broaden the utilization range, increasing the selectivity for CO in the syngas would be a significant development.

Previously, Chery *et al.* studied the nature of electrolytes Li_2CO_3–Na_2CO_3 (52 : 48 mol%), Li_2CO_3–K_2CO_3 (62 : 38 mol%), Na_2CO_3–K_2CO_3 (56 : 44 mol%), and a ternary mixture of Li_2CO_3–Na_2CO_3–K_2CO_3 (43.5 : 31.5 : 25 mol%) by thoroughly analyzing reoxidation and reduction.[27] Herein, the CO_2 reduction mechanism at a gold electrode in molten carbonates is investigated using cyclic voltammetry. The present work is a systematic exploration of changes in the H_2/CO ratio in various binary or ternary carbonates ($Li_{1.51}K_{0.49}CO_3$, $Li_{1.07}Na_{0.93}CO_3$, $Li_{1.43}Na_{0.36}K_{0.21}CO_3$, and $Li_{0.85}Na_{0.61}K_{0.54}CO_3$) mixed with LiOH that favor syngas formation, but inhibit metal deposition,[28] with the goal of broadening the H_2/CO ratio in syngas. During electrolysis, alkali oxides, which are produced from the decomposition of monovalent alkali carbonate and LiOH, can combine with CO_2 and H_2O to renew the electrolyte. This regeneration of the carbonate electrolyte affords an advantageous circulation system to give syngas as the final product of CO_2/H_2O reduction *via* co-electrolysis in molten salts. Furthermore, the electricity needed for this electrolysis is measured to assess whether electrolysis proceeds with a relatively high current efficiency. In this study, CO_2/H_2O is synergistically converted into valuable chemicals by electrolyzing molten salts, providing an alternative route to resolve global excessive CO_2 emissions and convert conventional electricity to chemical energy.

Experimental

Experimental methods

The electrolysis cell consists of an alumina crucible (Al_2O_3 > 99.9%, φ40 mm, 85 mm in height) filled with binary or ternary mixed carbonates ($Li_{1.51}K_{0.49}CO_3$, $Li_{1.07}Na_{0.93}CO_3$, $Li_{0.85}Na_{0.61}K_{0.54}CO_3$, and $Li_{1.43}Na_{0.36}K_{0.21}CO_3$) and LiOH for the CO_2/H_2O co-electrolysis experiments, with a total mixed molten salts mass of 80 g. The thermal energy for electrolysis was provided by a specially customized ceramic heating sleeve. Due to inevitable corrosion caused by the electrolytes and high-temperature oxidation, an affordable and corrosion-resistant electrode material was investigated for its long-term stability. Metallic materials Ni (φ1.6 mm, 39.7 cm in length, 20 cm^2, Hebei Steady Metal Products Co., LTD, China) and polished Fe (φ1.6 mm, 39.7 cm in length, 20 cm^2, Hebei Steady Metal Products Co., LTD, China), both in the form of spiral wires, were used as the anode and cathode, respectively. When the mixed salts reached the pre-set temperature, the two-electrode system was placed into the electrolyte and completely sealed with a sealant and sealing bolt. All electrolysis was performed in the voltage range 1.6–2.6 V. DC power (BK PRECISION 1715A) was used as the power supply for electrolytic production of carbon-based fuels in the electrolyte. The mean gas collection rate was near 120–140 mL min^{-1}, controlled by a volumetric flowmeter. The gaseous products were expelled into a sampling bag through a topside gas-guide tube under argon, which also protected the electroactivity of the electrode.

Table 1 Detailed operating conditions for electrolysis

Electrolyte	Temperature/°C	Voltage/V
$Li_{1.07}Na_{0.93}CO_3$–0.1LiOH	500	1.6, 1.8, 2.0, 2.2, 2.4, 2.6
	525	1.6, 1.8, 2.0, 2.2, 2.4, 2.6
	550	1.6, 1.8, 2.0, 2.2, 2.4, 2.6
	575	1.6, 1.8, 2.0, 2.2, 2.4, 2.6
	600	1.6, 1.8, 2.0, 2.2, 2.4, 2.6
$Li_{1.51}K_{0.49}CO_3$–0.1LiOH	500	1.6, 1.8, 2.0, 2.2, 2.4, 2.6
	525	1.6, 1.8, 2.0, 2.2, 2.4, 2.6
	550	1.6, 1.8, 2.0, 2.2, 2.4, 2.6
	575	1.6, 1.8, 2.0, 2.2, 2.4, 2.6
	600	1.6, 1.8, 2.0, 2.2, 2.4, 2.6
$Li_{1.43}Na_{0.36}K_{0.21}CO_3$–0.1LiOH	500	1.6, 1.8, 2.0, 2.2, 2.4, 2.6
	525	1.6, 1.8, 2.0, 2.2, 2.4, 2.6
	550	1.6, 1.8, 2.0, 2.2, 2.4, 2.6
	575	1.6, 1.8, 2.0, 2.2, 2.4, 2.6
	600	1.6, 1.8, 2.0, 2.2, 2.4, 2.6
$Li_{1.43}Na_{0.36}K_{0.21}CO_3$–0.1LiOH	500	1.6, 1.8, 2.0, 2.2, 2.4, 2.6
	525	1.6, 1.8, 2.0, 2.2, 2.4, 2.6
	550	1.6, 1.8, 2.0, 2.2, 2.4, 2.6
	575	1.6, 1.8, 2.0, 2.2, 2.4, 2.6
	600	1.6, 1.8, 2.0, 2.2, 2.4, 2.6

The molar ratio of hydroxide to carbonate in the LiOH and LiNa (LiK, LiNaK) eutectic electrolyte was defined as n_H:n_C. With n_H:n_C = 0.1 : 1, the experiments are performed at temperatures of 500–600 °C, with voltage of 1.6–2.6 V applied at each temperature. Table 1 shows the experimental electrolytic conditions in detail.

Product characterization

Afterwards, the syngas obtained from electrolysis was characterized by gas chromatography (GC, Agilent 7890B) equipped with a thermal conductivity detector (TCD) and hydrogen flame ionization detector (FID) to determine the content of each component. After obtaining the concentration of each substance from the chromatogram, only the cathode fuel gas (methane, hydrocarbons, hydrogen, and carbon monoxide) was calculated. Fourier transform infrared spectroscopy (FTIR, Tensor27) was used to characterize the molecular structure of the products. The current–voltage relationship of different cathode materials (0.5 cm^2 surface area) was measured using a Ni wire anode (20 cm^2 surface area). Additionally, the current efficiency was calculated from the charge (in Faradays) passed during electrolysis compared to the charge required to form each measured mole of the gaseous products using the following equation:[28]

$$\eta_i = 100 \times n_i \times (m_i/\mathrm{MW}_i) \times (\mathrm{Far}/Q) \quad (1)$$

where η_i is the current efficiency contributed by the "*i*-th" product (%), m_i is the mass of product *i* (g), MW_i is the molecular weight of product *i* (g mol^{-1}), and n_i is the number of electrons transferred per molecule of product *i*. Far is the charge

per mole of electrons (26.80 A h mol^{-1} = 96 485C mol^{-1}), and Q is the charge, calculated from I (A) × time (h).[28]

Results and discussion

Theoretical analysis of hydroxide selection

The reduction of CO_2/H_2O *via* co-electrolysis of a molten mixture of carbonates and hydroxide can be driven by applying an external force field to the electrolysis unit. As shown in Scheme 1, using a hermetic device, syngas and hydrocarbons are generated from the reaction of OH^- and CO_3^{2-} on the cathode surface, and oxygen is formed by oxidation of O^{2-} on the anode. The intermediate product (metal oxide) in the reaction process can absorb the incoming carbon dioxide and water, generating carbonates and hydroxides to regenerate the electrolyte, which completes the construction of a circulation system.

The target product, CO and H_2, can be obtained by the coelectrolysis of ionized OH^- and CO_3^{2-} *via* reaction (2). The generated O^{2-} can be consumed in the following two ways: (i) reaction with CO_2 or H_2O, regenerating CO_3^{2-} or OH^- according to reactions (3) or (4), and (ii) the oxidation of O^{2-} to produce oxygen *via* electron loss (reaction (5)).

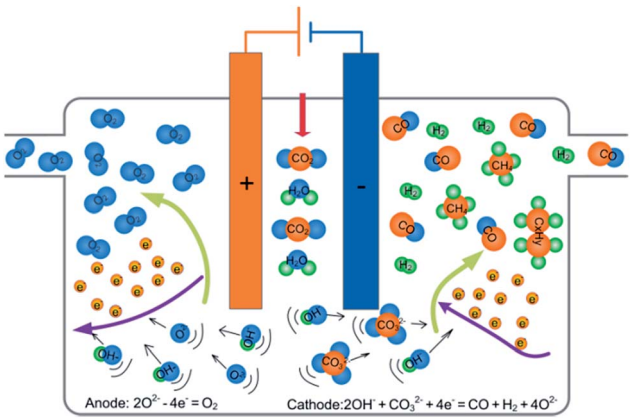

Scheme 1 Schematic diagram of experimental process.

$$2OH^- + CO_3^{2-} + 4e^- = CO + H_2 + 4O^{2-} \quad (2)$$

$$CO_2 + O^{2-} = CO_3^{2-} \quad (3)$$

$$H_2O + O^{2-} = 2OH^- \quad (4)$$

$$2O^{2-} - 4e^- = O_2 \quad (5)$$

The reacted OH^- in the electrolysis comes from hydroxide. It is necessary to control the source of OH^- to keep the produced syngas mixture at the desired H_2/CO ratio.

Compared to divalent molten salts, monovalent salts have higher conductivity, lower energy consumption, and give better electrical conductivity for the reduction of carbon dioxide at high temperature.[29,30] Basic data was obtained from NIST Chemistry WebBook[31] Fig. 1a shows the potential of metal deposition with three kinds of hydroxides. Unlike lithium hydroxide, pure sodium or potassium hydroxide tended to reduce the alkali cation to the alkali metal because of the relatively low metal deposition potentials. When KOH serves as the hydrogen source, K metal required a lower potential than H_2, meaning that K metal deposition could become a side reaction.[32] Fig. 1b shows the calculated thermodynamic electrolysis potential of various hydroxides as a function of temperature for syngas formation. The electrolysis potential was calculated from the thermochemical enthalpy and entropy of individual species. The formulae can be written as:[33]

$$E^\circ = -\Delta G^\circ/n \times \mathrm{Far} \quad (6)$$

$$\Delta G^\circ(T) = \sum \nu_B H^\circ(B,T) - T \times \sum \nu_B S^\circ(B,T) \quad (7)$$

$$H^\circ - H_{298.15}{}^\circ = A \times t + B \times t^2/2 + C \times t^3/3 + D \times t^4/4 - E/t + F - H \quad (8)$$

$$S^\circ = A \times \ln(t) + B \times t + C \times t^2/2 + D \times t^3/3 - E/(2 \times t^2) + G \quad (9)$$

where ν_B is the stoichiometric number, B is a component of the reaction, H° is the standard enthalpy (kJ mol^{-1}), S° is the standard entropy (J mol^{-1} K^{-1}), G° is the standard Gibbs free

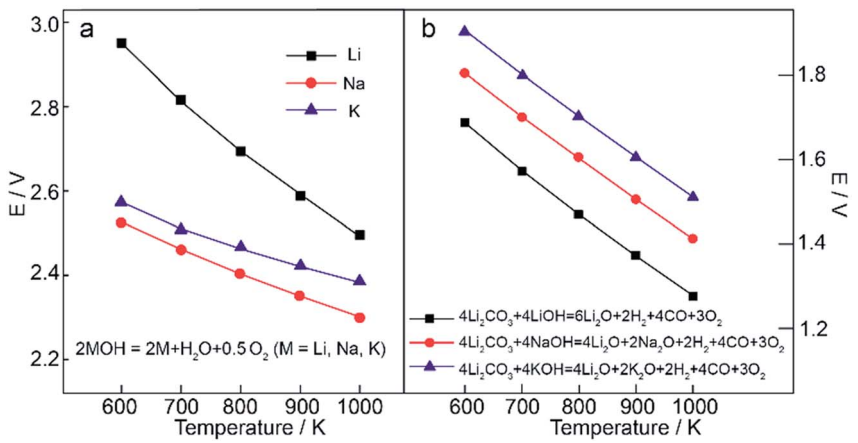

Fig. 1 Calculated thermodynamic potential of (a) metal deposition and (b) syngas generation in different hydroxide systems.

energy (kJ mol^{-1}), Far is the Faraday constant (96 485C mol^{-1}), n is the number of transferred electrons, $t = T/1000$, and T is the temperature in K, and A–G are thermodynamic parameters.[33]

For ease of discussion, the absolute value of the electrolysis potential was used to represent the calculation value. As shown in Fig. 1b, the theoretical electrolytic voltage in the equations of various MOH (M = Li, Na, K) for syngas generation decreased with increasing electrolytic temperature. At 700 K, the energy required for syngas production corresponded to a voltage of 1.57 V in the LiOH electrolyte, which was lower than those in NaOH electrolyte (1.70 V) and KOH electrolyte (1.80 V). In comparison to the NaOH and KOH systems, the LiOH system required a lower potential, and Li deposition was relatively low. As the KOH system showed contrary behavior at the same electrolytic temperature, the LiOH electrolyte was chosen as the optimal system.

Determination of optimal temperature and operating voltage

The eutectic points of pure lithium, sodium, or potassium carbonates are 723, 851, and 891 °C, respectively. The relatively high melting temperature of the individual carbonates increases both the reaction energy consumption and heat loss. Low carbonate melting points are achieved by eutectic mixtures of alkali carbonates, such as $Li_{1.51}K_{0.49}CO_3$, $Li_{1.07}Na_{0.93}CO_3$, $Li_{0.85}Na_{0.61}K_{0.54}CO_3$ and $Li_{1.43}Na_{0.36}K_{0.21}CO_3$ at 490, 499, 375, and 390 °C, respectively.[34–36] To achieve the controlled synthesis of syngas at relatively low temperatures, a binary carbonate mixture of Li–Na or Li–K or a ternary carbonate mixture of Li–Na–K were chosen as electrolytes to reduce the reaction temperature in this study. The highest eutectic point of the electrolytes studied was 499 °C ($Li_{1.07}Na_{0.93}CO_3$) and the lowest eutectic point of the electrolytes studied was 375 °C ($Li_{0.85}Na_{0.61}K_{0.54}CO_3$). As interpreted in our previous study, a high electrolysis temperature leads to an increased hydrogen yield due to enhanced reactivity.[28] Due to slower ionic migration, poor conductivity at low electrolytic temperature, difficulty of operation, and corrosion resistant performance at a high operating temperature, an appropriate temperature range was shown to be necessary for stable, continuous, and efficient electrolysis. Furthermore, according to previous theoretical and electrochemical reports, the selective electroreduction of CO_2 to CO likely occurs in Li–Na and Li–K molten salts at ≤650 °C by cyclic voltammetry.[37,38] Furthermore, temperatures of over 600 °C favor methane formation, achieving a methane yield of 64.9% in a eutectic mixture of carbonates as electrolyte in electrochemically reducing H_2O/CO_2.[28] In our previous study,[33] when the temperature was about 550 °C, the methane content was less than 25%. After conducting a systematic experimental study of experimental data, the range of electrolysis temperatures studied herein was chosen as 500–600 °C.

The electrolytic voltages required to form the reduction products in various reactions were calculated using the Gibbs energy at temperatures ranging from 400 K to 900 K in molten lithium carbonate. As shown in Fig. 2, obvious downward trends were observed for cathodic product generation. Beyond that, theoretical calculation also demonstrated that electrolysis

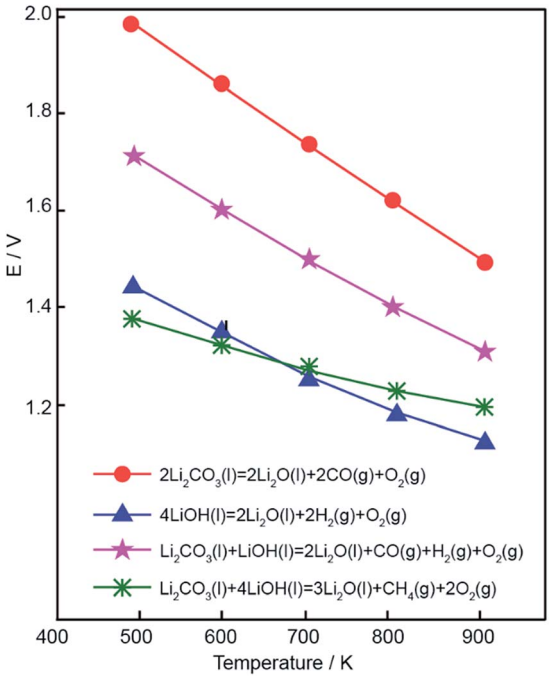

Fig. 2 Required electrolysis potentials of possible reactions at various temperatures.

voltage was another critical factor for controlling reaction selectivity. The electrolysis temperatures investigated ranged from 773 K to 873 K, and the electrolytic potential of the mixtures of carbonates and hydroxide further decreased. Therefore, the potentials of pure lithium carbonate decomposition were below 1.6 V. However, 1.6 V was taken as the starting voltage in this study because of the concentration overpotential, electrochemical overpotential, and resistance overpotential.[39,40] The actual decomposition voltage was greater than the theoretical value, E(decomposition potential) = E(theory decomposition voltage) + E(overpotential) + IR. According to our previous study,[32,33] metal deposition occurs at higher voltages and, when the voltage exceeds 2.5 V, the CO content showed a significant downward trend. Therefore, an electrolysis voltage range of 1.6–2.6 V was determined.

Optimization of electrodes for molten carbonate/hydroxide conversion

In $Li_xNa_yK_zCO_3$–LiOH electrolytes, O_2 is produced from the oxidation of O^{2-} and CO_3^{2-} at the anode, according to reactions (5) and (10):

$$2CO_3^{2-} - 4e^- = 2CO_2 + O_2 \quad (10)$$

To prevent electrolyte corrosion and high-temperature oxidation of these ions, a cost-effective and corrosion-resistant electrode material with long-term stability is necessary. In our previous study, a Ni electrode showed a lower anodic overpotential by polarization analysis.[28] Therefore, Ni wire was used as the anode in this electrochemical study. To select cathode materials with excellent chemical stability, Ni, Fe, and Ni–Cr

were tested as applicable cathodes. The electrochemical performance of these materials was evaluated using polarization tests, as shown in Fig. 3.

As the current density increased, the overpotential also increased, and the working voltage of the electrolytic cell exceeded the rest potential voltage. Minimizing this overpotential was essential to achieve maximum energy efficiency during electrolysis. The lowest cathodic overpotential and low cost made Fe a preferable cathode material. Therefore, a Fe cathode was a viable choice for long-term electrolysis in Li_2CO_3–Na_2CO_3–K_2CO_3/LiOH. We believe that the low overpotential observed for the Fe cathode presents an analogous electrocatalytic opportunity for syngas production *via* simultaneous splitting of hydroxide and carbonate on a similar surface. Therefore, iron and nickel were selected as the cathode and anode materials, respectively.

Analysis and characterization of electrochemical products

Gaseous products prepared from the $Li_{0.85}Na_{0.61}K_{0.54}$–0.1LiOH electrolyte at a temperature of 550 °C, using 20 cm^2 of Fe wire as the cathode and 20 cm^2 of Ni wire as the anode, were monitored by gas chromatography (GC) and IR spectroscopy. Gas chromatography detection consisted of a hydrogen flame ionization detector (FID) and thermal conductivity detector (TCD). As shown in Fig. 4a (FID), small by-products, such as propane and *n*-butane, were generated during electrolysis. TCD signals also indicated a small amount of CH_4, and these alkanes are collectively represented as C_xH_y. The presence of CO, H_2, and the anodic product were also shown in the TCD signals. As shown in Fig. 4b, peaks in the range 3000–3100 cm^{-1} were associated with unsaturated C–H stretching vibrations,[41,42] while peaks from 2800 cm^{-1} to 3000 cm^{-1} clearly indicated saturated C–H stretching vibrations, including –CH_3 and –CH_2–. Trace amounts of CO_2 were present in the gaseous products. CO_2 has four modes of vibration, with two being infrared-active. The presence of CO_2 was confirmed by the stretching vibrations

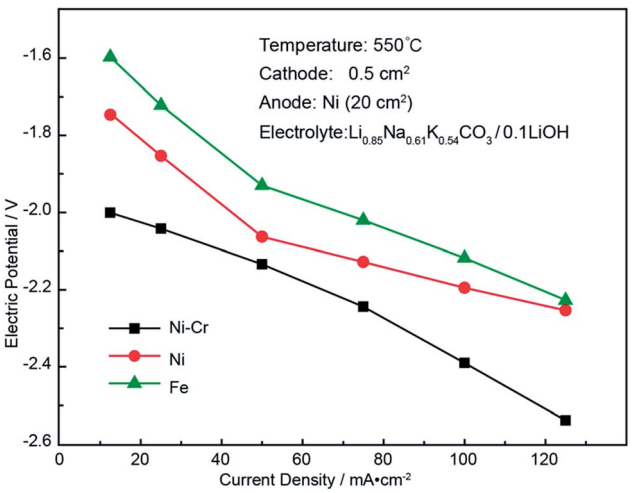

Fig. 3 Polarization curves of various cathode materials during electrolysis.

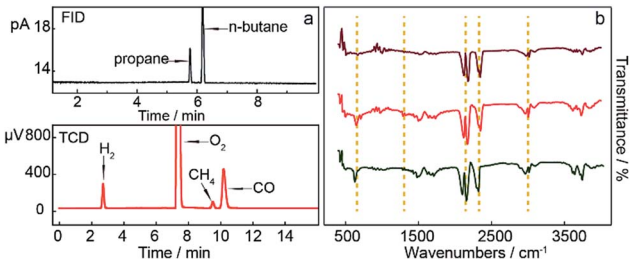

Fig. 4 Results of gaseous product analysis from (a) gas chromatograph with FID and TCD, and (b) IR spectra under the same electrolytic conditions.

at 2349 cm^{-1} and the flexural vibration at 667 cm^{-1}.[43] The stretching vibration of C≡O was present in the range 2200–2250 cm^{-1}, which proved the presence of CO. The peaks from 1300–1400 cm^{-1} corresponded to C–H bending vibrations, and peaks from 1300–1700 cm^{-1} were associated with C–C stretching vibrations. The peaks at around 750 cm^{-1} corresponded to C=C out-of-plane flexural vibrations in *cis*-olefins. The above IR observations demonstrated that the products of CO_2/H_2O coelectrolysis contained a large amount of CO and hydrocarbons in this work.

Effect of mixed molten carbonate compositions on syngas product selectivity

As shown in Fig. 5, under all investigated electrolytic temperatures with voltage ranging from 1.6 V to 1.8 V, CO was the main product. However, a further increase in applied voltage (1.8–2.6 V) seemed to favor H_2 generation, indicating that 1.8 V resulted in the optimum CO fraction. To illustrate the dependence of syngas composition on temperature, CO, H_2, and C_xH_y fractions at 1.8 V were calculated at five temperatures, as shown in Fig. 6.

Fig. 6 shows the gaseous product contents in the $Li_{1.07}$-$Na_{0.93}CO_3$–0.1LiOH system at various electrolytic temperatures. When the applied temperature was increased from 500 to 550 °C, the CO content increased gradually under the same electrolysis voltage. For instance, the yield of CO rose from ~43.2% at 500 °C and 1.8 V to ~55.7% at 550 °C and 1.8 V. In contrast, under the same electrolysis conditions, the H_2 content gradually decreased with increasing electrolysis temperature (500–550 °C), showing that increasing temperature led to an increase in current density and favored CO generation. As the electrolysis temperature was further increased (550–600 °C), the H_2 content increased gradually while the CO content gradually decreased at the same electrolysis voltage. This could be ascribed to the reduction potential required by H_2 and CO decreasing at elevated temperature. However, the rate of decrease in H_2 production was faster than that of CO, meaning that 550 °C was the optimum electrolysis temperature for this system. This result showed the dependence of the CO fraction on the applied temperature, with higher temperatures found to not favor targeted CO production. The change in C_xH_y byproduct content was within 10%. The above-mentioned experimental results showed that 550 °C was the optimum electrolysis temperature for the Li–Na system. Specifically, the H_2/CO

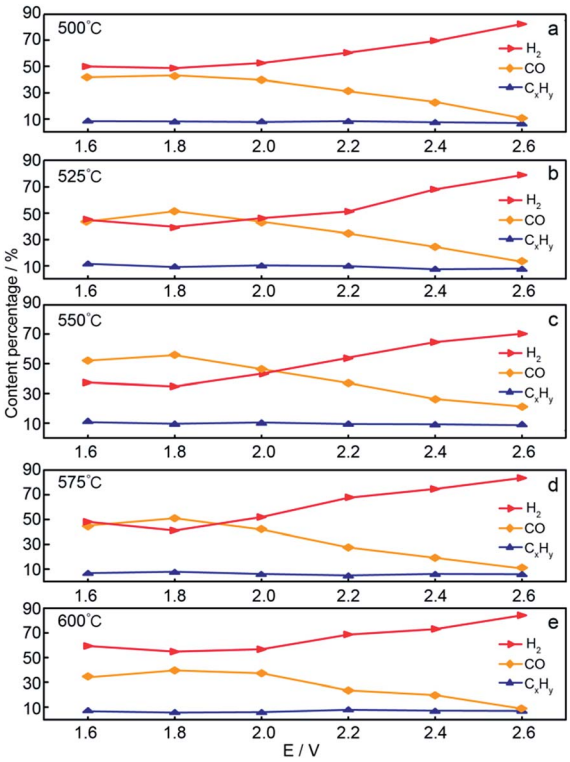

Fig. 5 Compositions of electrolysis gaseous products in the operating voltage range 1.6–2.6 V at temperatures of 500 °C, 525 °C, 550 °C, 575 °C, and 600 °C in the $Li_{1.07}Na_{0.93}CO_3$–0.1LiOH electrolyte system.

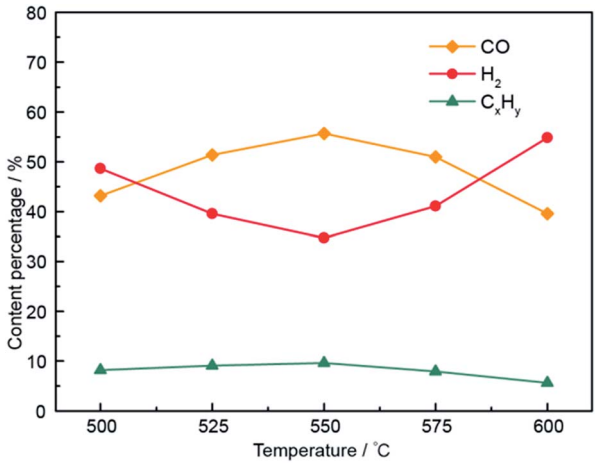

Fig. 6 Compositions of electrolysis gaseous products at temperatures of 500–600 °C in the $Li_{1.07}Na_{0.93}CO_3$–0.1LiOH electrolyte system.

molar ratio of 0.62–9.60 was gained by adjusting the electrolysis voltage and operating temperature of the Li–Na system. Compared with previous research,[23–25] syngas was generated simultaneously with a H_2/CO ratio of less than 1.

Selection of the optimum electrolytic voltage for the $Li_{1.51}K_{0.49}CO_3$–0.1LiOH system is shown in Fig. S1.† At 1.6 V, the CO content increased with increasing electrolysis temperature (500–550 °C), as shown in Fig. 7, indicating that the solubility of CO_2 increased with elevating temperature and the kinetics were

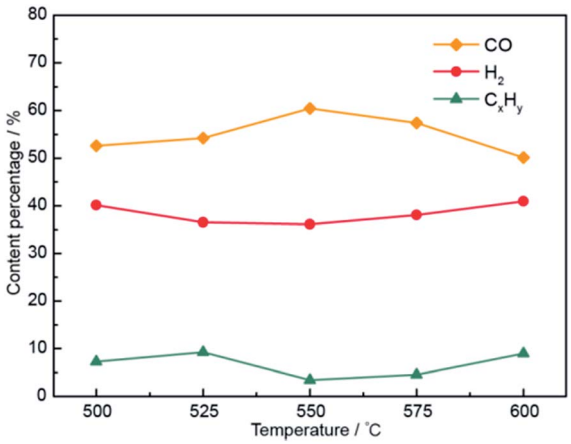

Fig. 7 Compositions of electrolysis gaseous products at temperatures of 500–600 °C in the $Li_{1.51}K_{0.49}CO_3$–0.1LiOH electrolyte system.

enhanced.[44,45] The CO content decreased with a further increase in temperature (550–600 °C). This might be attributed to CO oxidation occurring at 575 °C in the Li–K system.[22] This showed that the best electrolysis temperature for the Li–K system was 550 °C. As shown in Fig. S1,† the H_2/CO molar ratios were well controlled in the range 0.76–5.04, 0.67–8.08, 0.59–4.33, 0.66–4.04, and 0.81–4.07. In particular, the adjustable range of H_2/CO molar ratio range in the $Li_{1.51}K_{0.49}CO_3$–0.1LiOH system was 0.59–8.08.

Selection of the optimum electrolytic voltage for the $Li_{1.43}Na_{0.36}K_{0.21}CO_3$–0.1LiOH system under electrolytic temperatures is shown in Fig. S2,† and a detailed description can be found in the ESI.† Fig. 8 plots the gas concentration of the $Li_{1.43}Na_{0.36}K_{0.21}CO_3$–0.1LiOH system at various temperatures. The CO concentration by electrolysis at 1.8 V in $Li_{1.43}Na_{0.36}K_{0.21}CO_3$–0.1LiOH increased to ~61.6% as the electrolytic temperature was increased from 500 °C to 550 °C, indicating that the increase in the temperature favored the formation of CO. Concurrently, at the applied voltage of 1.8 V, the hydrogen concentration dropped to ~32.8%, and other products stayed at around ~5%. The CO content then gradually declined at temperature of 550–600 °C, while the hydrogen content increased with increasing temperature (550–600 °C). This phenomenon was caused by high-temperature activation of the $Li_{1.43}Na_{0.36}K_{0.21}CO_3$ electrolyte and hydrogen formation was due to the activity of growth[32] The CO content of the system reached a maximum of ~61.7% while the H_2 content was 32.8% at 1.8 V and 550 °C. The adjustable range of the H_2/CO molar ratio was 0.53–7.76 in the Li_2CO_3–Na_2CO_3–K_2CO_3 system with a mass ratio of 61 : 22 : 17.

Selection of the optimum electrolytic voltage for the $Li_{0.85}Na_{0.61}K_{0.54}CO_3$–0.1LiOH system has also been interpreted in Fig. S3.† At an electrolysis voltage was 2.2 V, the compositions of the electrolysis gaseous products are shown in Fig. 9. The CO content gradually increased, the H_2 content gradually decreased, and the CO selectivity increased slightly when increasing the temperature from 500 to 550 °C. With a further increase in temperature, the CO content began to decrease, while the H_2 content gradually increased. With a lower

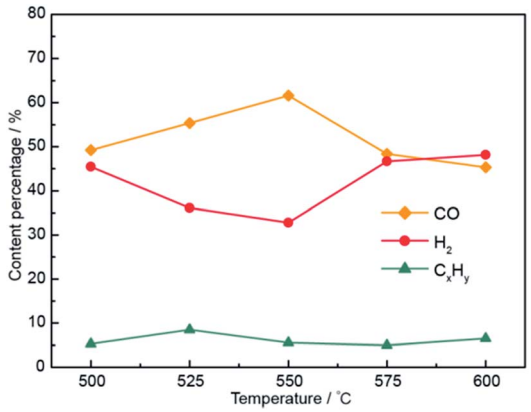

Fig. 8 Compositions of electrolysis gaseous products at temperatures of 500–600 °C in the $Li_{1.43}Na_{0.36}K_{0.21}CO_3$–0.1LiOH electrolyte system.

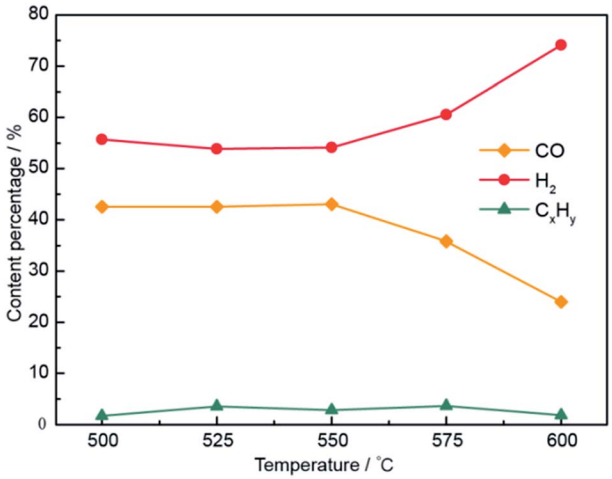

Fig. 9 Compositions of electrolysis gaseous products at temperatures of 500–600 °C in the $Li_{0.85}Na_{0.61}K_{0.54}CO_3$–0.1LiOH electrolyte system.

electrolysis potential required for the temperature rise, the higher temperature did not contribute to CO formation. These results confirmed that the CO content reached a maximum at 550 °C and 2.2 V. The H_2/CO molar ratio was 1.02, and the H_2/CO molar ratio ranged from 1.02 to 7.42 in $Li_{0.85}Na_{0.61}K_{0.54}CO_3$ by tuning the voltage and temperature.

In summary, the four electrolyte systems investigated presented varying H_2/CO molar ratio ranges under different electrolytic conditions, but with the common feature that all maximum CO fractions were observed at 550 °C. This was a desirably low temperature (*vs.* 800 °C)[22] that could lead to the highly efficient one-pot generation of syngas by CO_2/H_2O *via* coelectrolysis in molten salts. In detail, compared with $Li_{0.85}Na_{0.61}K_{0.54}CO_3$–0.1LiOH, the other three systems demonstrated an advantage in the generated H_2/CO ratio, implying an enlarged application potential. Furthermore, $Li_{1.51}K_{0.49}CO_3$–0.1LiOH and $Li_{1.43}Na_{0.36}K_{0.21}CO_3$–0.1LiOH provided maximum CO contents of more than 60%, which were superior to those of $Li_{1.07}Na_{0.93}CO_3$–0.1LiOH and $Li_{0.85}Na_{0.61}K_{0.54}CO_3$–0.1LiOH. Therefore, it was concluded that a larger Li_2CO_3 fraction favored CO generation, and that Li_2CO_3-induced modification at the interface between the cathode and electrolyte might be responsible for the observed changes in CO contents. By regulating the composition of the electrolytes, the synthesis of wide range of H_2/CO ratios has been successfully realized, and the industrial application range of syngas has been expanded.

Current efficiency is a significant metric of CO_2/H_2O transformation selectivity. Regarding the volume of obtained gaseous products, the current efficiency was calculated, as shown in Fig. 10. An irregular change in the current efficiency was observed in the $Li_{1.07}Na_{0.93}CO_3$–0.1LiOH and $Li_{1.51}K_{0.49}CO_3$–0.1LiOH systems, and the current efficiency of each reduction product was lower than 60%. Presumably, this was due to the deposition of alkali metals at the cathodic surface.[46] CO_3^{2-} ions can also be reduced indirectly *via* the prior reduction of alkali metal ions to the metal (reactions (11) and (12)).[47]

$$M^+ + Xe^- \rightarrow M \quad (11)$$

$$4M + M_2CO_3 \rightarrow C + 3M_2O \quad (12)$$

In another study on a Ni electrode under similar conditions to that stated earlier, the cathodic limit corresponded to the reduction of CO_3^{2-} ions to carbon, while the anodic limit was assigned to the oxidation of Ni according to reaction (13).[48]

$$Ni^{2+} + 2e^- \rightarrow Ni \quad (13)$$

Of the four electrolytes investigated, the mixture of $Li_{0.85}Na_{0.61}K_{0.54}$–0.1LiOH exhibited a higher current efficiency

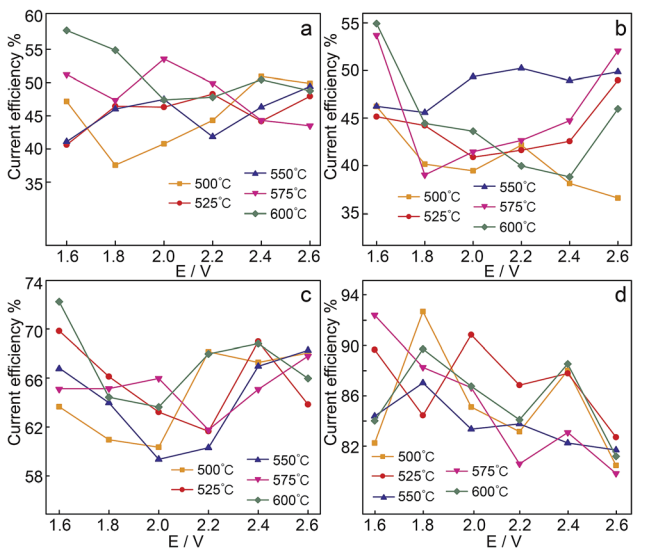

Fig. 10 Current efficiencies of total gas generation in various electrolytes measured in the two-electrode system (a) $Li_{1.51}K_{0.49}CO_3$–0.1LiOH electrolyte system, (b) $Li_{1.51}K_{0.49}CO_3$–0.1LiOH electrolyte system, (c) $Li_{1.43}Na_{0.36}K_{0.21}CO_3$–0.1LiOH electrolyte system, (d) $Li_{0.85}Na_{0.61}K_{0.54}$–0.1LiOH electrolyte system.

with an optimum efficiency approaching ~93%. However, it produced a relatively low fraction of CO (~25%). The current efficiencies for fuel gas production are all over 79%, signifying that regulating applied cell voltages leads to syngas generation of various concentrations.

Conclusions

In summary, the one-pot generation of syngas with a wide range H_2/CO ratios (0.62–9.6 *vs.* over 1) was achieved through rationally designed molten salt electrolysis system. Electrolysis was carried out at 500–600 °C with an operating voltage of 1.6–2.6 V using a low-cost Fe cathode and Ni anode. CO_2/H_2O was directly transformed into syngas *via* electrolysis in the $Li_{0.85}Na_{0.61}K_{0.54}$–0.1LiOH electrolyte, with a 93.2% current efficiency at a constant voltage of 1.8 V and temperature of 500 °C. Moreover, the molar ratios of H_2/CO were 0.62–9.60, 0.59–8.08, 0.53–7.76, and 1.02–7.42 for $Li_{1.07}Na_{0.93}CO_3$–0.1LiOH, $Li_{1.51}K_{0.49}CO_3$–0.1LiOH, $Li_{1.43}Na_{0.36}K_{0.21}CO_3$–0.1LiOH, and $Li_{0.85}Na_{0.61}K_{0.54}$–0.1LiOH electrolytes, respectively. Syngas with diverse H_2/CO ratios was obtained by regulating the electrolyte composition, applied cell voltage, and electrolytic temperature. The methane-based hydrocarbon content varied by within 10% in the four electrolytes. In this manner, this work provides a path for further enhancements of product selectivity of CO and H_2, and demonstrates a new sustainable process for recycling H_2O and CO_2.

Conflicts of interest

There are no conflicts to declare.

Acknowledgements

This work is supported by the National Natural Science Foundation of China (No. 21476046 and 21306022), the Specialized Research Fund for the Doctoral Program of Higher Education of China (No. 20132322120002), the China Postdoctoral Science Foundation (No. 2013M540269), the Postdoctoral Science Foundation of Heilongjiang Province of China (No. LBH-TZ0417), and partly supported by the Science Foundation for Creative Research Groups of the Heilongjiang Higher Education Institutes of China (No. 2013TD004) and the Northeast Petroleum University (No. SJQHB201602 and YJSCX2016-018 NEPU).

Notes and references

1 B. Kumar, M. Llorente, J. Froehlich, *et al.*, *Annu. Rev. Phys. Chem.*, 2012, **63**, 541.
2 W. K. Fong, H. Matsumoto, C. S. Ho and Y. F. Lun, *Planning Malaysia Journal*, 2008, **6**, 101.
3 D. C. Grills, Y. Matsubara, Y. Kuwahara, *et al.*, *J. Phys. Chem. Lett.*, 2014, **5**, 2033.
4 J. R. Bolton and D. O. Hall, *Annu. Rev. Energy*, 1979, **4**, 353.
5 R. Wick and S. D. Tilley, *J. Phys. Chem. C*, 2015, **119**, 26243.
6 Q. Kong, D. Kim, C. Liu, *et al.*, *Nano Lett.*, 2016, **16**, 5675.
7 D. R. Kauffman, J. Thakkar, R. Siva, *et al.*, *ACS Appl. Mater. Interfaces*, 2015, **7**, 15626.
8 W. H. Wang, Y. Himeda, J. T. Muckerman, *et al.*, *Chem. Rev.*, 2015, **115**, 12936.
9 C. Costentin, M. Robert and J. M. Savéant, *Acc. Chem. Res.*, 2015, **48**, 2996.
10 H. K. Lim, H. Shin, W. A. Goddard, *et al.*, *J. Am. Chem. Soc.*, 2014, **136**, 11355.
11 M. Azuma, K. Hashimoto, M. Hiramoto, M. Watanae and T. Sakata, *J. Electrochem. Soc.*, 1990, **137**, 1772.
12 F. Köleli, T. Atilan, N. Palamut, *et al.*, *J. Appl. Electrochem.*, 2003, **33**, 447.
13 C. W. Li and M. W. Kanan, *J. Am. Chem. Soc.*, 2012, **134**, 7231.
14 A. Więckowski, E. G. M. Szklarczyk and J. Sobkowski, *Electrochim. Acta*, 1983, **28**, 1619.
15 H. Wu, Z. Li, D. Ji, Y. Liu, *et al.*, *RSC Adv.*, 2017, **7**, 8467.
16 Y. Matsuzaki and I. Yasuda, *J. Electrochem. Soc.*, 2000, **147**, 1630.
17 H. Yang, Y. Gu, Y. Deng and F. Shi, *Chem. Commun.*, 2002, **2002**, 274.
18 H. Wu, Z. Li, D. Ji, Y. Liu, *et al.*, *Carbon*, 2016, **106**, 208.
19 M. E. S. Hegarty, A. M. O'Connor and J. R. H. Ross, *Catal. Today*, 1998, **42**, 225.
20 M. S. Rana, V. Sámano, *et al.*, *Fuel*, 2007, **8**, 1216.
21 R. Dvořák, T. Pařízek, L. Bébar, *et al.*, *Clean Technol. Environ. Policy*, 2009, 95.
22 Y. Liu, D. Ji, Z. Li, D. Yuan, *et al.*, *Int. J. Hydrogen Energy*, 2017, **42**, 18165.
23 T. Riedel, M. Claeys, H. Schulz, *et al.*, *Appl. Catal., A*, 1999, **186**, 201.
24 J. H. Lee, K. Y. Koo, U. H. Jung, *et al.*, *Korean J. Chem. Eng.*, 2016, **33**, 3115.
25 F. Sastre, M. J. Muñoz-Batista, *et al.*, *ChemElectroChem*, 2016, **3**, 1497.
26 N. Tien-Thao, M. H. Zahedi-Niaki, *et al.*, *Appl. Catal., A*, 2007, **326**, 152.
27 D. Chery, V. Albin, A. Meléndez-Ceballos, *et al.*, *Int. J. Hydrogen Energy*, 2016, **41**, 18706.
28 H. Wu, D. Ji, L. Li, D. Yuan, *et al.*, *Adv. Mater. Technol.*, 2016, **1**, DOI: 10.1002/admt.201600092.
29 D. J. Adams, T. M. Dwyer and B. Hille, *J. Gen. Physiol.*, 1980, **75**, 493.
30 S. B. Kausley, C. P. Malhotra and A. B. Pandit, *Journal of Water Process Engineering*, 2017, **16**, 149.
31 *NIST Chemistry WebBook. NIST Standard Reference Database Number 69*, ed. P. J. Linstrom and W. G. Mallard, National Institute of Standards and Technology, Gaithersburg, MD, 2016, http://webbook.nist.gov.
32 D. Ji, Y. Liu, Z. Li, *et al.*, *Int. J. Hydrogen Energy*, 2017, **42**, 18156.
33 H. Wu, Y. Liu, D. Ji, *et al.*, *J. Power Sources*, 2017, **362**, 92.
34 C. W. Bale and A. D. Pelton, *CALPHAD: Comput. Coupling Phase Diagrams Thermochem.*, 1982, **6**, 255.
35 S. Licht, *Adv. Mater.*, 2011, **23**, 5592.
36 S. Licht, H. Wu, Z. Zhang and H. Ayub, *Chem. Commun.*, 2011, **47**, 3081.

37 D. Chery, V. Albin, V. Lair and M. Cassir, *Int. J. Hydrogen Energy*, 2014, **39**, 12330.
38 D. Chery, V. Lair and M. Cassir, *Electrochim. Acta*, 2015, **160**, 74.
39 J. J. Yang, C. H. Choi, H. B. Seo, H. J. Kim and S. G. Park, *Electrochim. Acta*, 2012, **86**, 277.
40 H. Li and C. Oloman, *J. Appl. Electrochem.*, 2005, **35**, 955.
41 C. Kötting, J. Güldenhaupt and K. Gerwert, *Chem. Phys.*, 2012, **396**, 72.
42 P. Grimaldi, L. D. Giambattista, S. Giordani, *et al.*, *Spectrochim. Acta, Part A*, 2011, **84**, 74.
43 C. H. Lin and H. Bai, *Ind. Eng. Chem. Res.*, 2004, **43**, 5983.
44 Y. Kanai, K. Fukunaga, K. Terasaka, *et al.*, *Chem. Eng. Sci.*, 2013, **100**, 153.
45 H. Gupta and L. S. Fan, *Ind. Eng. Chem. Res.*, 2002, **41**, 4035.
46 H. V. Ijije, R. C. Lawrence and G. Z. Chen, *RSC Adv.*, 2014, **4**, 35808.
47 M. L. Deanhardt, K. H. Stern and A. Kende, *J. Electrochem. Soc.*, 1986, **133**, 1148.
48 F. Lantelme, B. Kaplan, H. Groult and D. Devilliers, *J. Mol. Liq.*, 1999, **83**, 255.